Desalination and Water Treatment
www.deswater.com

doi: 10.1080/19443994.2016.1173381

57 (2016) 23293–23307
October

Taylor & Francis
Taylor & Francis Group

Effect of cell hydrodynamics in desalination of saline water by sweeping air pervaporation technique using innovated membrane

Mahmoud M. Elewa[a], Ahmed A. El-Shafei[b,*], Abeer A. Moneer[c,*], Mona M. Naim[d]

[a]*Research and Development Department, Arab Academy for Science, Technology and Maritime Transport, Alexandria, Egypt, email: mahmoud.elewa@gmail.com*
[b]*Faculty of Agriculture, Agricultural and Biosystems Engineering Department, Alexandria University, Alexandria, Egypt, Tel. +20 100 6159433; email: ahmed.elshafi@alexu.edu.eg*
[c]*Marine Pollution Department, Marine Environmental Division, National Institute of Oceanography and Fisheries, Alexandria, Egypt, Tel. +20 122 2590830; email: yrwah@yahoo.com*
[d]*Faculty of Engineering, Chemical Engineering Department, Alexandria University, Alexandria, Egypt, email: monanaim66@gamil.com*

Received 31 May 2015; Accepted 28 February 2016

ABSTRACT

Scarcity of potable water nowadays, presents a serious problem all over the world. Environmental changes are taking place at a rapid pace, resulting in greenhouse effects, desertification, and lack of fresh water. Accordingly, scientists are working hard toward inventing new techniques for desalinating sea water, which presents the only alternative solution to this problem. In this regard, desalination techniques are mainly divided into thermal and membrane techniques. However, the latter are superior in that they are modular in shape, and consume less energy. In the present work, desalination by a novel recent membrane separation technique, the so-called sweeping air pervaporation (PV), which has been very sparsely applied to desalination of sea water, has been conducted in our laboratory. The technique is simple, straightforward, cost-effective and does not suffer from limitations as regards low water recovery, such as reverse osmosis. An innovated deacetylated cellulose acetate (CA) membrane was prepared by the phase inversion technique, from a specially formulated casting solution mixture composed of CA, acetone (A), dioxane (D), dimethyl formamide, dimethyl phthalate, and maleic anhydride in definite proportions, and used in all the experiments. Two PV cells of different configuration and aspect ratio (AR) were designed and constructed, in order to investigate the effect of hydrodynamics on membrane performance. Numerous variables were studied for their effect on the pervaporate flux (J) and % salt rejection (%SR), and these were: initial salt solution concentration (C_i), PV temperature (Tpv), and PV cell configuration. It was found that the flux obtained was directly proportional to Tpv, and that the J was almost independent of C_i at low Tpvs, except in the case of Tpv = 80°C for both small and large configurations, where J was inversely proportional to C_i (in the range 15–120 g/l), and that higher fluxes were obtained under the same conditions in case of the PV cell of higher AR. The activation energy (E_a) for

*Corresponding authors.

Presented at EuroMed 2015: Desalination for Clean Water and Energy Palermo, Italy, 10–14 May 2015. Organized by the European Desalination Society.

permeation through the membrane in both the cells was computed from the Arrhenius equation, and was found to be 20.89–23.06 kJ/mol K at C_i = 120 g/l, for the cell with higher and lower AR, respectively, denoting facile permeation of water through the membrane, for the two cell designs, in particular with higher AR. The results indicate that at all concentrations tested for large cell below 70˚C, the product, after a once-through operation, was exceptional potable water with very low salinity (%SR 98.9) even when C_i was 120.8 g/l, and maximum flux obtained was 5 l/m^2 h at Tpv = 70˚C. The separation factor (α), PV separation index (PSI), overall mass transfer coefficient (K_{ov}), diffusion coefficient (D_i), salt diffusivity (D_s), and salt permeability (P), through the membrane were all calculated and their values are stated inside the paper text. Nevertheless, α varied between 5.6 and 853.4, and PSI reached 3494.5 l/m^2 h.

Keywords: Desalination; Sweeping air pervaporation; Deacetylated cellulose acetate membrane; Cell hydrodynamics; Mass transfer

1. Introduction

Water is the most vital resource for life. Fresh river water supplies typically rely on capturing surface waters, which have recently dropped below record levels, mainly due to greenhouse effect and global warming. It is prospected that water in the few coming years, will present a real problem worldwide, and is actually on the verge of triggering wars among nations [1]. Many areas around the world, such as numerous African countries, suffer from fresh water deficiency, for both drinking and irrigation, as well as for industrial purposes. Therefore, people in such areas, are compelled to rely on desalination of either brackish or sea water and/or sources of highly contaminated water for their living. Thus, desalinating sea water is expected to take on greater significance [2]. It has been estimated that the annual water volume used by industry, will increase to 50% above 1995 levels, by 2025 [3].

Desalination of sea water relieves the dependence on unpredictable rain and snowfalls, and allows for a more dependable supply from the seemingly endless ocean resource. Nowadays, the most commonly used techniques to produce fresh water from sea water by desalination, are mainly multistage flash or reverse osmosis (RO) [4]. However, numerous other novel desalination processes are lately emerging, which require minimum energy and lowest investment costs. One of the techniques which fulfill both these requirements, as well as simplicity in operation, and less tendency to membrane fouling due to permeation of vapor, instead of water as is the case with RO, is the youngest member in the membrane separations family pervaporation (PV) [5]. The latter is presently considered as a well-established membrane separation technique with high potential, particularly in the dehydration of alcohols and breaking of azeotropes [5]. However, it is now being considered for desalination [6–9]. In PV, the dependence of the overall solute flux on the flow regime stems from the laminar boundary layer adjacent to the membrane surface where, at dilute concentration of the solute in the feed solution, transport occurs solely by diffusion [10]. The performance of a PV membrane is commonly evaluated by two experimental parameters, namely the permeation flux (J) and selectivity. Selectivity can be generally expressed in two different ways of which the separation factor (α) is one common representation of selectivity [10]. The PV separation index (PSI) in kg m^{-2} h^{-1} is another way to define the separation ability of a membrane [11].

Polymers are the main membrane materials for PV because of their high process ability and outstanding permselectivity. Of those cellulose acetate (CA), followed by PVA, are conventional commercial membrane materials. CA is a natural and renewable material with superior film forming ability, and is widely used for separation of organic mixtures by PV [12], and in desalination by RO, while PVA is a highly hydrophilic polymer with high flexibility and abrasion resistance, and exhibits acceptable water permselectivity in pervaporative dehydration of organics [13–15].

Cho et al. [16] have achieved ion rejection of over 99.9% combined with a water flux of 1.9 kg/m^2 h at 69˚C for synthetic sea water tested using a NaA zeolite membrane. Ultrapure water has also been produced from North Sea water using a hydroxyl sodalite PV membrane with ion rejection greater than 99.99% [17]. Although the mechanism of transport and ion rejection remains controversial, several research groups have established that PV through zeolite membranes shows great promise for desalination applications [1,7,18,19]. Currently, the most popular zeolite membranes for PV applications are synthetic thin-film zeolite membranes supported on porous substrates [1,6–9,16–20]. Several major factors restrict their application to industrial desalination, however, including strict requirements for the structural properties of the

support materials. Poor chemical and physical compatibility between the available support materials and the zeolite layer increases the cost of production and the presence of defects formed during membrane preparation. Other concerns, including fragile thin surface layers and tedious synthesis procedures, also reduce the feasibility of applying thin-film membranes. Hydrophilic ion-exchange membranes based on sulfonated polyethylene hollow fibers were manufactured by Korin et al. [21], the membranes' suitability for a water PV process was studied for possible application in water desalination. In a study by Korngold and Korin [22], air sweep water PV through a hydrophilic anion-exchange hollow fiber membrane and through a porous hydrophobic hollow fiber was investigated.

Ben Hamouda et al. [23] prepared hydrophobic dense PEBAX membrane and their suitability for desalination of brine by PV was studied. The effects of brine inlet temperature (28–54˚C) and NaCl concentration in the feed brine (0–3.5 mol l^{-1}) were determined. A water flux of 1.3–7 g m^{-2} h^{-1} was obtained using this type of membranes. The authors found that the optimal specifications for their membrane was a thickness of 100 μm and an operating temperature of 50˚C that provide a water flux of 7 g m^{-2} h^{-1} in the permeate side. Quiñones-Bolaños et al. [24] studied the suitability of a homogeneous hydrophilic dense membrane in PV, for reusing brackish and/or contaminated waters. Xie et al. [25] prepared hybrid polymer-inorganic membranes by cross-linking PVA, maleic acid (MA), and silica via an aqueous sol–gel route. Zwijnenberg et al. [26] described details of a solar driven PV process for the production of desalinated water from highly contaminated waters. Drobek et al. [27], prepared Silicalite-1 (S-1) and ZSM-5 membranes by secondary growth on tubular ceramic supports which were tested using a PV setup for the desalination of aqueous solutions containing NaCl in concentrations corresponding to brackish (0.3–wt.%), sea (3.5 wt.%) and brine (7.5–15 wt.%) water. The pervaporative salts rejection and water flux characteristics of the NaA zeolite membrane in sea water were investigated by Cho et al. [16], The upper limit of the non-zeolitic pore diameter was 8 Å. Liang et al. [28] prepared a three-layer thin-film nano-fibrous PV composite (TFNPVC) membrane by sequential deposition using electrospraying/electrospinning. Heat treatment is believed to be an important step in controlling the morphology and properties of polymer-based membranes. In a study by Xie et al. [29], hybrid organic–inorganic membrane based on PVA, MA, and tetraethyl orthosilicate (TEOS) was synthesized via a sol–gel route.

Sweeping air PV is simpler than vacuum PV, and there is limited literature citing the application of separations by PV using sweeping air, particularly desalination. In case of vacuum PV, the costs are much higher than in the case of sweeping air as regards to the necessity of liquid nitrogen which is costly and not safe to use in the condensation step, and it is also more complicated compared to sweeping air in which air is available at no cost and condensation is effected at 0–2˚C (using only an ice-water bath).

The aim of the present work is to fabricate an innovated membrane suitable for desalination by PV and to study the effect of heating temperature of saline solution (Tpv), initial concentration of saline solution (C_i), configuration and aspect ratio of the PV cell, and the cell hydrodynamics, on the flux (J), salt rejection (%SR), the separation factor (α), PV PSI, activation energy (E_a), overall mass transfer coefficient (K_{ov}), diffusion coefficient (D_i), alt diffusivity (D_s), and salt permeability (P) through the membrane.

2. Materials and methods

2.1. Materials

CA (Gomhouria Company, Egypt), Acetone (A) (El Nasr Pharmaceutical Chemicals, Egypt), Dimethyl phthalate (DMP) (Koch-light laboratories Ltd, Colnbrook Bucks, England), Dimethyl formamide (DMF) (Vebjenapharm Laborchemie Apolda, Germany), Dioxane (D), Maleic anhydride (MA) (SN, SCO. Chemicals), sodium chloride (El Nasr Salines company, Egypt), and sodium hydroxide (Chemajet Chemical Company, Egypt) were all used as such in all the experiments.

2.2. Methods

2.2.1. Preparation of casting solution

CA powder and MA powder were added to a wide-mouthed glass-stoppered bottle, then dissolved in a mixture of solvents including DMF, D, A, and DMP in different weight proportions. The mixture was mixed manually using a glass rod until all the CA dissolves, then the membrane solution was left overnight, in the tightly sealed bottle, until complete removal of air bubbles.

2.2.2. Casting of membranes

The solution was cast on a smooth uniform glass plate of a casting assembly equipped with a doctor's

blade, then was immersed in distilled water contained in a tray, for 60 min, to effect coagulation, during which the membrane changed from transparent color to white. It was detached slowly from the glass sheet and steeped in a distilled water bath, ready for deacetylation.

2.2.3. Deacetylation of membranes

The membranes were subjected to complete deacetylation by steeping them for 24 h in an aqueous alkaline bath consisting of 1% sodium hydroxide and 20% sodium chloride, at room temperature. The membranes were then washed by repetitive steeping in distilled water followed by decantation then stored in distilled water for later use in the PV experiments.

2.2.4. Pervaporation test cells

Two test cells of different configurations were devised and constructed, and are described in the following section:

2.2.4.1. Small cell. The cell consisted of two identical plexiglass parallel-piped halves. Each cell half contained a compartment consisting of hexagonal grooves (length 12.2 cm, width 5.5 cm, and depth 0.5 cm as shown in Fig. 1) containing numerous lateral corrugations to induce slight turbulence (if any) of the flowing liquid on the feed side of the membrane, and enhances mass transfer by partial elimination of the boundary layer. Before operation, the two cell halves were firmly held together with a set of six bolts and nuts such that the membrane completely separated the two halves. Rubber gaskets placed all around the grooves functioned as liquid seals and prevented leakage during PV. The cell was then clamped horizontally, ready for operation.

2.2.4.2. Large cell. This cell was basically similar in idea to the small cell, but the dimensions were totally different, as regards length, width, and depth of the grooves, which were 20.2, 4.4, and 1.5 cm, in respective order as shown in Fig. 1. However, there were no internal lateral corrugations, owing to the large depth of the flow path.

2.2.5. Experimental setup

Fig. 2 illustrates a schematic diagram of the setup which consists of the PV cell, feed solution flask, electric heater, and saline-water pump, constituting the heating circuit; and a cooling water pump, a long Liebig condenser, and an ice-water bath, constituting the cooling circuit. The last once-through route is that of the purge air provided by an air blower, which sweeps the permeating vapor from the downstream of the cell and forces it to pass through the condenser, where it is condensed into water drops that are collected in a receiver flask.

2.2.6. Procedure

The PV membrane was placed in the test cell, then the latter was closed tightly by the bolts and nuts, placed horizontally and the whole unit was connected. Two liters of sodium chloride solution were heated to the required temperature, and allowed to recycle through the top compartment of the cell. The pump and blower were operated, and the condensate was collected at hourly intervals, in the receiving flask, and analyzed for concentration by a conductivity meter, and its volume measured. The solution temperature was also recorded every hour. Recycling of the solution ensured constancy of its temperature adjacent to the membrane, which at the same time, together with the corrugations (of the small cell) eliminated the laminar boundary layer next to the membrane, minimized concentration polarization and enhanced mass transfer through the membrane. Each experiment was conducted for six hours at least, after which the experiment was terminated. It is noteworthy that the flow rate across the membrane in the small cell was 2.4 times that in the large cell.

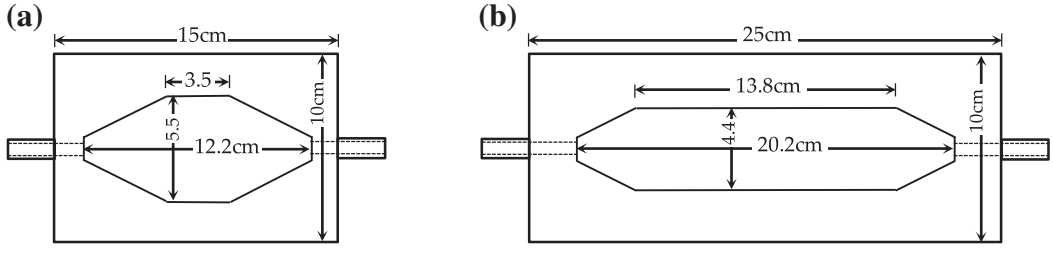

Fig. 1. A schematic diagram of (a) small PV cell and (b) large PV cell.

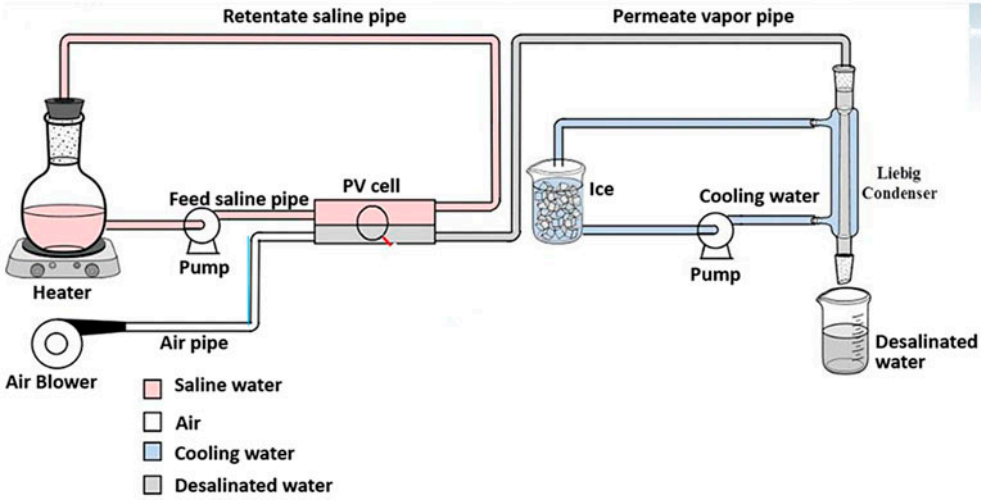

Fig. 2. A schematic of the pervaporation (PV) setup.

2.2.7. Membrane characterization

Fourier transform infrared (FT-IR) of membrane was obtained by the FT-IR spectroscopy (VERTEX 70, Bruker Co., Germany). Water contact angle was measured to evaluate the hydrophilicity of the membrane surface. The static contact angles of water on the membrane surface were measured by contact angle goniometer (JC-2000C Contact Angle Meter, Power each Co., Shanghai, China). The average value of static contact angle on membrane was calculated with at least five different locations on membrane. The surface and cross section morphology of membrane were examined using scanning electron microscopy, SEM, (JOELJSM 6360 LA, Japan).

2.2.8. PV membrane performance

Performance of PV membrane is determined by the values of J, %SR, α, and PSI as follows, in which:

$$J = \frac{Q}{A \cdot t} \tag{1}$$

where Q is the volume of the permeate collected in time t, A is the effective membrane area,

$$\%\mathrm{SR} = \frac{C_\mathrm{i} - C_\mathrm{f}}{C_\mathrm{i}} \times 100 \tag{2}$$

where C_i and C_f are the initial and final solution concentration,

$$\alpha = \frac{Y_w/Y_s}{X_w/X_s} \times 100 \tag{3}$$

where Y and X are the weight of components in the pervaporate and feed, respectively, the suffix w refers to water and s refers to solute, and

$$\mathrm{PSI} = J \times \alpha \tag{4}$$

2.2.9. Activation energy (E_a)

The dependence of flux on Tpv could be expressed by Arrhenius law as follows and from which E_a could be computed:

$$J = A_\mathrm{p} \exp\left(-\frac{E_\mathrm{a}}{RT}\right) \tag{5}$$

where A_p, R, and T are the pre-exponential factor, universal gas constant, and feed temperature in absolute units, respectively. E_a is determined from the plot of ln J vs. $1/T$. A linear relationship is produced from which E_a is computed from the slope of the straight line.

2.2.10. Mass transfer

In a batch recycle PV experiment, the overall mass transfer coefficient (K_ov) was computed from the following [30]:

$$K_{ov} = \frac{V}{A\,t} \ln \frac{C_0}{C_t} \tag{6}$$

where V is the volume of saline solution in the feed flask, A is the membrane area subjected to PV and C_t and C_0 are the solute concentrations at time t and time equals zero, respectively.

2.2.11. Salt transport properties

The apparent diffusion coefficient (D_i) of water was determined from the following equation derived from Fick's law:

$$D_i = \frac{J\delta}{C_i} \tag{7}$$

where δ is the membrane thickness and C_i is the concentration of water at the membrane feed side.

Transport of NaCl in membrane was assessed by kinetic desorption experiments. The NaCl diffusivity (D_s) in the membrane was determined based on a Fickian analysis [31] as follows:

$$D_s = \frac{\pi\delta^2}{16}\left[\frac{d(M_t/M_\infty)}{d(t^{1/2})}\right]^2 \tag{8}$$

where M_t is the total amount of NaCl extracted from the membrane at time t, M_∞ is the total amount of NaCl extracted from the membrane at long times, and $d(M_t/M_\infty)/d(t^{1/2})$ is the slope of the linear portion of M_t/M_∞ as a function of $t^{1/2}$.

The NaCl distribution coefficient, K_s, was calculated from the amount of salt extracted and the concentration of the original solution as follows:

$$K_s = \frac{\text{g NaCl/cm}^3 \text{ membrane}}{\text{g NaCl/cm}^3 \text{ solution}} \tag{9}$$

The NaCl permeability coefficient (P) was calculated by the product of K_s and D_s [31], i.e.:

$$P = K_s D_s \tag{10}$$

3. Results and discussion

3.1. FT-IR spectra and contact angle of the fabricated membrane

Fig. 3 illustrates the FT-IR spectra of the PV membrane, from which it is clear that the membrane has OH functional group (3,000–3,750 m^{-1}). Besides the typical hydroxyl group which makes the membrane superhydrophilic due to the presence of three OH groups per anhydroglucose unit, the additional peak 1,640–1,630 m^{-1} clarifies the adsorption of water, which assist not only in the make and break of hydrogen bonding of water but also causing easy permeation of water across the membrane. In addition, the peak at 1,125–1,170 m^{-1} which attributed to C–O–C asymmetric stretching vibration (arabinose side chain), while the peak at 1,040–1,050 m^{-1} assigned to C–O stretching in C–O–C glycosidic bonds, which both confirmed the existence of the ether linkages between the anhydroglucose units and the asymmetric stretch of the arabinose side chain. It has also been verified that none of the solvents/additives were retained in the membrane matrix and that they were leached out during coagulation and post-washing. This observation has been studied by Naim et al. [32], in which the membrane was cast from only cellulose acetate and acetone as solvent, and on comparing the FT-IR of this membrane and other membranes included more solvents/additives; it is confirmed that they have the same peaks which proves that all solvents were totally leached out.

The contact angle of the fabricated membrane gave 0°, where the water molecules are strongly attracted to the membrane molecules, and the water drops were completely spread out on the solid surface. Accordingly, the result emphasizes the superhydrophilic nature of our membrane.

3.2. Effect of the initial concentration on membrane performance

Results of the present work are illustrated in the following Figs. 4–7, in which Figs. 4 and 5 depict the effect of C_i on J and %SR at different Tpv, respectively, in the two cells of different configurations tested. The first figure shows that in general, J is in direct proportionality with Tpv in the two cells investigated, and that J is higher in case of the large cell with higher aspect ratio, and deeper cross section of flow. Also in the majority of cases, J decreases as C_i increases, which is a known fact that J usually decreases as C_i increases, or at best interest remains constant. Accordingly, this result must be attributed to the cell design and its aspect ratio, as well as to thickness of the flow cross section. It seems that a higher aspect ratio and a wider cross section both contribute to turbulence of the saline solution as it flows through the cell length, which helps in preventing concentration polarization next to the membrane surface, by

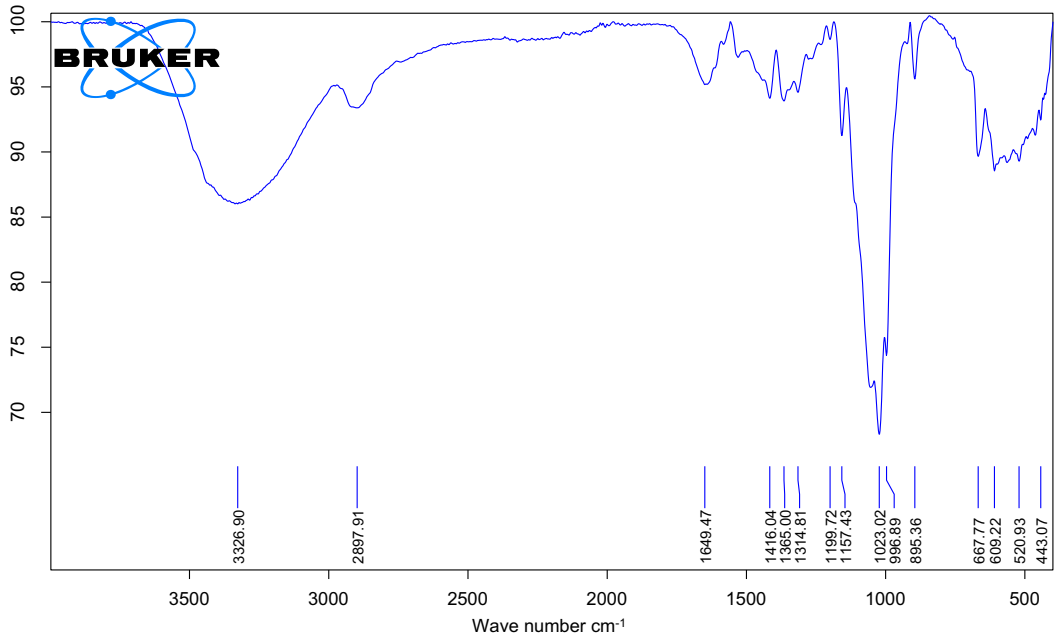

Fig. 3. FT-IR spectra of fabricated membrane.

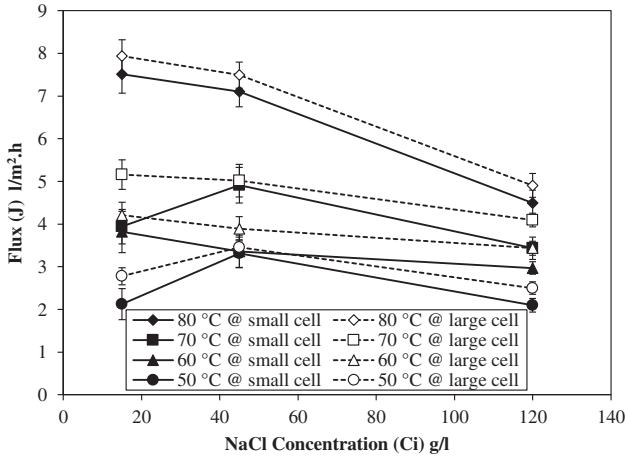

Fig. 4. Effect of initial feed concentration on flux at different PV temperatures and different cell aspect ratios.

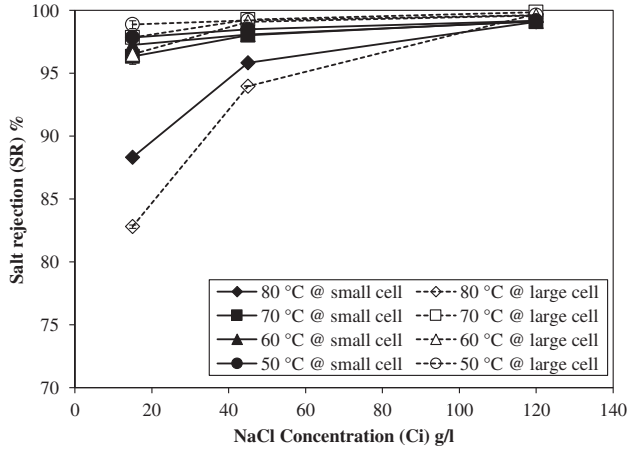

Fig. 5. Effect of initial feed concentration on salt rejection at different PV temperatures and different cell aspect ratios.

renewal of the solution adjacent to the membrane. Conclusively, it can be stated that a higher cell aspect ratio and a deeper cross-section are preferred to its counterpart. However, the fluxes are almost comparable to those reported by Liang et al. [28] and Korngold et al. [33], despite that in the two cases lower C_{is} were applied. However, it is noteworthy that the techniques applied were very cumbersome and sophisticated equipment including electro-spraying and electro-spinning techniques were required in a sequential three-stage process in the first case, in which the thickness of each layer was hard to control, in addition to the continuous loss of the electro-spun PAN layer. As to the technique applied by Korngold et al. [33], it included a complicated and expensive process which required sulfochlorination, amination followed by quaternization of ready-made polyethylene hollow fibers. In contrast, our membrane was fabricated by a very direct, simple and cheaper method.

However, the effect of C_i on %SR at different Tpv is clarified in Fig. 5. The figure shows that %SR

generally increases with increase in C_i, so that at $C_i = 120$ g/l, %SR is 99.1 at all Tpv tested. Interestingly, it is observed that the increase in %SR is pronounced with increase in C_i, at the highest Tpv tested, and becomes less and less pronounced as Tpv decreases from 80 to 50˚C. Moreover, the %SR is lower in case of the large cell at the lowest concentration and the highest Tpv (80˚C); however, it becomes the highest at all C_{is} tested, at the lowest Tpv (50˚C), compared to the small cell. It is noteworthy that salt rejection at 15 g/l and at 80˚C compared to the same results at higher concentrations at the same temperatures is low; that is because the difference between initial concentration and pervaporate concentration is considered low compared to that obtained at higher concentrations. At 80˚C, concentration of pervaporate at 15 g/l for small cell was 1.75 g/l (Table 1), and at 120 g/l and under the same conditions, was 1.1 g/L, which are very near results to each other. It is clear that %SR increases as Tpv decreases, and as C_i increases which may be attributed to the unique configuration of the PV cell and its large aspect ratio, which provides turbulence at the membrane surface, causing eddies that prevent concentration polarization in particular, and results in flux increase and a concomitant improvement in salt rejection.

It is worth mentioning that the best performance from the authors' point of view was achieved, using the large cell, at Tpv = 70˚C, for C_i from 15, 45 to 120 g/l, at which the %SR was high and equivalent to a final pervaporate concentration from 0.322, 0.335 to 0.148 g/l, while the fluxes were 5.16, 5.01, and 4.1 l/m^2 h, respectively. Once again, this proves that cell configuration has a profound influence on the membrane performance. This result is very promising in that exceptionally high %SR is obtained at 120 g/l at all Tpv tested. Thus, this membrane can be used in membrane crystallization operations whereby saline solutions can be initially concentrated to very high concentrations, prior to crystallization.

In Fig. 6 which clarifies the effect of C_i on α at the four Tpv investigated, for both cells, it is clear upon meticulous inspection, that the large cell provides a much higher α, which increases almost exponentially with C_i, so that at 120 g/l, α at 70˚C is around 850, while it is only around 130 at the same C_i at all Tpv tested, for the small cell. This is a unique phenomenon, which may be attributed to the following

Table 1
Diffusion mass transfer and salt transport properties

Cell size	C_i (g/l)	Tpv (˚C)	Cpv (g/l)	J (l/m^2 h)	$D_i \times 10^{-4}$ cm^2/s	$K_{ov} \times 10^{-9}$ cm/s	$D_s \times 10^{-7}$ cm^2/s	$P \times 10^{-9}$ cm^2/s
Large cell	15	50	0.1694	2.78	7.72	4.18	6.26	7.07
	15	60	0.5225	4.21	11.69	6.96	3.82	13.31
	15	70	0.3215	5.16	14.33	8.35	1.44	3.08
	15	80	2.5786	7.94	22.05	11.14	4.87	83.73
	45	50	0.3626	3.46	3.20	5.57	2.55	2.06
	45	60	0.4118	3.89	3.60	6.96	2.62	2.40
	45	70	0.3346	5.01	4.64	8.35	2.90	2.16
	45	80	2.7060	7.49	6.94	11.14	7.81	46.99
	120	50	0.4621	2.50	0.87	4.18	13.53	5.21
	120	60	0.4159	3.44	1.19	5.57	29.64	10.27
	120	70	0.1481	4.09	1.42	6.96	5.64	1.19
	120	80	0.3584	4.91	1.70	8.35	20.61	3.84
Small cell	15	50	0.3226	2.12	3.54	0.79	0.38	0.82
	15	60	0.4107	3.82	6.36	2.36	1.35	3.69
	15	70	0.5477	3.94	6.57	2.36	2.99	10.90
	15	80	1.7521	7.51	12.51	3.15	1.20	14.06
	45	50	0.6785	3.31	1.84	1.58	2.07	3.12
	45	60	0.8688	3.35	1.86	1.58	0.69	1.34
	45	70	0.8886	4.91	2.73	2.36	0.76	1.50
	45	80	1.8686	7.10	3.95	3.15	2.77	11.51
	120	50	0.9872	2.10	0.44	0.79	2.10	1.73
	120	60	1.0490	2.97	0.62	1.58	2.25	1.97
	120	70	1.0351	3.43	0.72	1.58	2.41	2.10
	120	80	1.1000	4.50	0.94	2.36	2.69	2.46

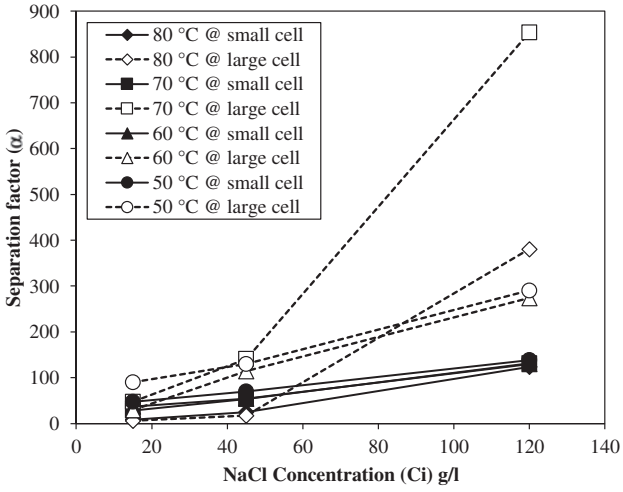

Fig. 6. Effect of initial feed concentration on separation factor at different PV temperatures and different cell aspect ratios.

reasons: as the solution flows transversally in cross flow through the cell, it is subjected to restricted flow at the outlet, which causes part of the liquid to divert its direction causing turbulence in the deep cross section of the cell, and unsteady flow results. This phenomenon leads to renewal of the surface adjacent to the membrane, evading concentration polarization, and allowing much more water, free from salt, to permeate through the asymmetric superhydrophilic membrane. On the other hand, flow is streamline in the small cell, so at the surface of the membrane, the liquid is more or less stagnant, as a result, concentration polarization is excessive in comparison to the other case, and greatly influences the value of α, in that salt is compelled to permeate with the water, owing to its presence in high concentration in the vicinity of the membrane's surface. However, it remains to be mentioned that the previous discussion emphasizes the governing effect of this behavior in case of the small cell, in that Tpv has no effect on α, since as water pervaporates through the membrane, it takes a proportionate quantity of salt with it from the stagnant boundary layer, in the form of solvated ions, irrespective of the Tpv. It is noteworthy that the least α was obtained at the lower C_i (15–45 g/l) for the large cell, at Tpv = 80˚C, whereas the highest value was obtained, for the same cell, at the highest C_i studied (120 g/l), at 70˚C, which may be attributed to the pronounced contrasting effects C_i and Tpv have on the water flux, being inversely and directly proportional to C_i and Tpv, respectively, thereby making the ratio of water to salt in the permeate largest at the highest Tpv tested (80˚C), and lowest at the highest C_i tested (120 g/l).

Fig. 7 illustrates the effect of C_i on PSI, from which it is observed that the curves tend to take a similar pattern as those of Fig. 6, which is expected. Accordingly, the core discussions of Fig. 6 apply to the present figure as well. However, the values of PSI range from as low as 50 to as high as 3,500, which proves as mentioned earlier why most researchers do not rely on PSI in evaluating membrane performance, as mentioned in the discussion of Fig. 6, for the value of PSI is not very indicative, as is, α, or flux, since a membrane offering a very high flux with a modest α can give the same value of PSI as another with a modest flux and a very high α, the PSI in these two cases being merely acceptable.

At any rate, when PSI is very high as in our case, the membrane is certainly of high performance, in desalination by PV, since both α and flux must be acceptably high.

3.3. Effect of PV temperature on membrane performance

Fig. 8 shows the effect of Tpv on the J at three different C_i. It is clear that the J varies directly with temperature, as expected, due to increased diffusivity of water. However, the salt is effectively rejected by the membrane skin layer, as demonstrated in the previous figure. It is noticed that the minimum J was obtained when C_i was 120 g/l and when the small cell of lowest aspect ratio was used, as found earlier. On the other hand, the highest J's were obtained when C_i was 15 g/l, and using the large cell.

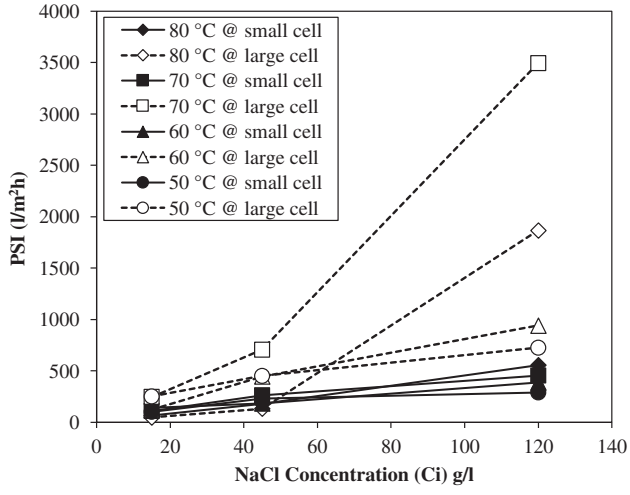

Fig. 7. Effect of initial feed concentration on PV separation index (PSI) at different PV temperatures and different cell aspect ratios.

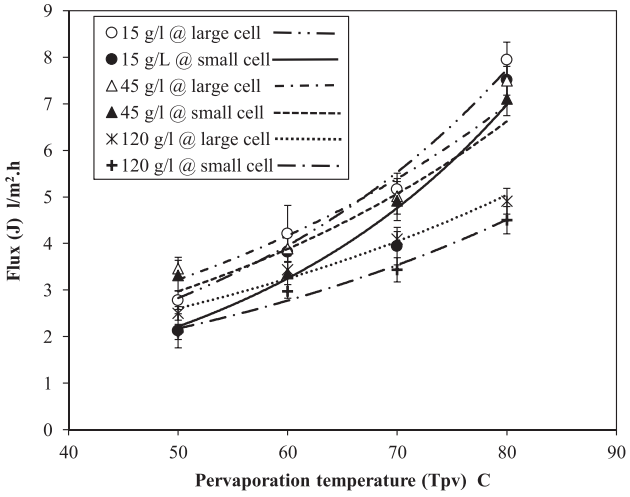

Fig. 8. Effect of PV temperatures on flux at different initial feed concentrations and different cell aspect ratios.

The next figure (Fig. 9) depicts the effect of Tpv on %SR for different C_i. It is clear that %SR is in all cases higher than 96.4, except at 80˚C at which it varied from 82.8 to 99.7 as C_i increased from 15 to 120 g/l, at which %SR was higher in case of the large cell rather than the small cell. It is observed that the maximum %SR takes place when $C_i = 120$ g/l, independent of temperature, which can be attributed to the hydrophilic character of the membrane, being a perfectly asymmetric membrane with an optimum skin layer that rejects the salt (as will be shown later); however, some concentration polarization surely takes place, which must be responsible for reduction in water flux, concomitantly, preventing salt permeation through the membrane.

It must be noted that the salt molecules are surrounded by a sheath of water, which assists in increasing its permeation with pervaporating water, the latter increasing as Tpv increases. Therefore, this explains why %SR increases with Tpv, in that more water permeation competes with the salt, delaying its passage through the membrane.

The effect of Tpv on the separation factor (α) at different C_i is illustrated in Fig. 10. It is observed that α is almost independent on Tpv, producing almost horizontal lines at the three C_{is} studied. However, α varies directly with C_i, being in the thereabouts of 290–853 at 120 g/l for the large cell. Additionally, the values of α are higher in case of the larger cell under all the conditions shown in the figure. It is worth noting that the maximum α takes place when $C_i = 120$ g/l at the Tpv = 70˚, since the α is calculated from pervaporate and initial concentrations (Eq. (3)), and since the concentrations of the pervaporate (Cpv) are very small and almost equal to each other for all the experiments carried out for this membrane at different conditions of temperature and initial concentration (Table 1). On the other hand, the results above 70˚C indicate that the membrane suffers from opening out of the pores (stretching) at higher temperatures, which lead to low salt rejection and higher flux simultaneously, than those below this temperature. At 70˚C, the concentration of the pervaporate is the lowest at all temperatures (below and above this temperature) especially for the large cell, which was 0.148 g/l compared to other results ranging at about 0.4 g/l; this led to increasing the value of separation factor from 290

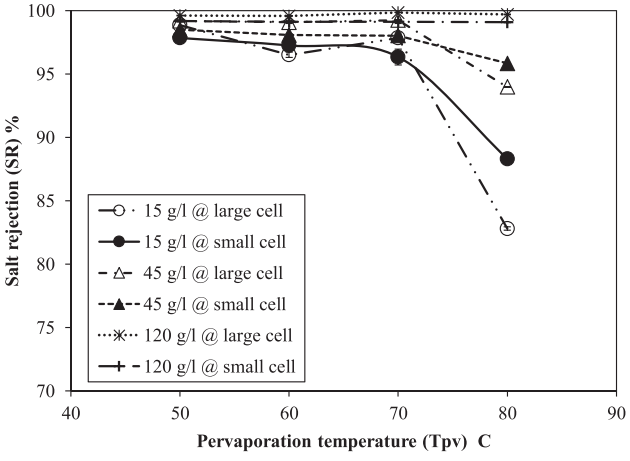

Fig. 9. Effect of PV temperatures on slat rejection at different initial feed concentrations and different cell aspect ratios.

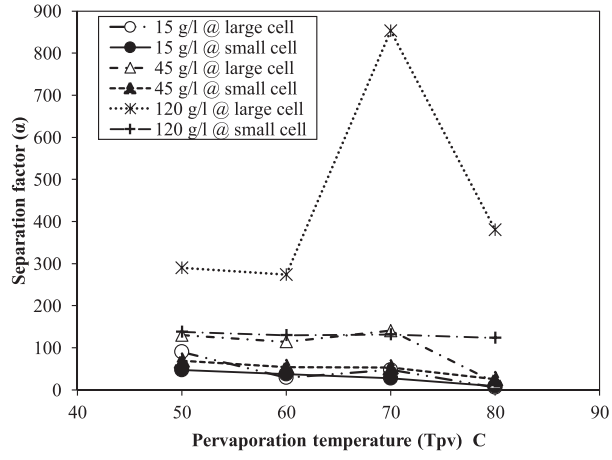

Fig. 10. Effect of PV temperatures on separation factor at different initial feed concentrations and different cell aspect ratios.

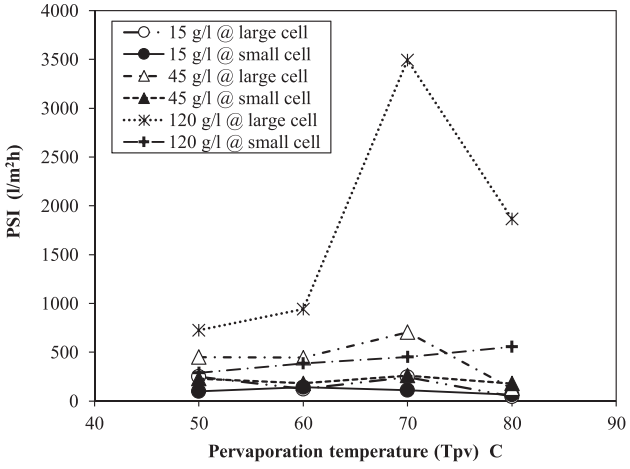

Fig. 11. Effect of PV temperatures on PV PSI at different initial feed concentrations and different cell aspect ratios.

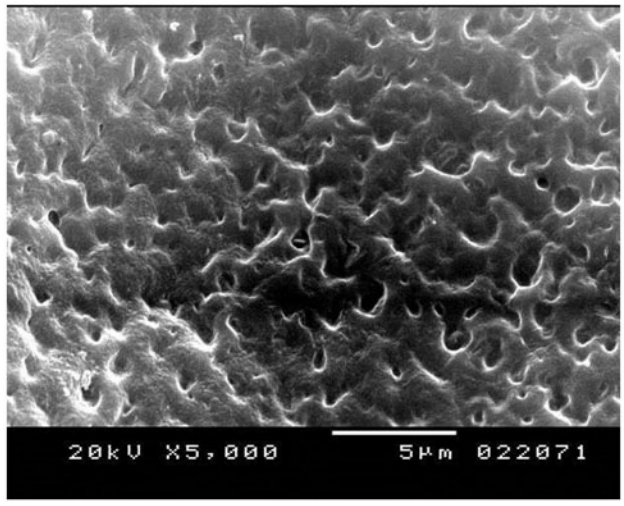

Fig. 12. SEM surface micrograph of fabricated membrane with magnification of 5,000×.

to 853. Naim et al. [34] found that the results above 70°C followed the same trend as the obtained results in the present work, which proves that PV is preferable to be used at temperatures up to 70°C and below 80°C, which is an advantage for this process economically.

Fig. 11 shows the effect of Tpv on the PV PSI at the same C_i used in the previous figure, from which the same aforementioned discussions on the effect of Tpv on α generally apply (lowest four curves). However, it is worth noting that PSI reached the vicinity of 3,495 l/m^2 h at the Tpv tested (70°) and when C_i was equal to 120 g/l, using the large cell.

Moreover, the curves at 120 g/l increase almost linearly with Tpv, for both cells, which was primarily due the high separation factors (see Fig. 10), followed by the high fluxes (see Figs. 4 and 8), at high Tpv, which gave a high product ($J \times \alpha$). However, the value of PSI is not very indicative, as is, α or flux, since a membrane offering a very high flux with a modest α can give the same value of PSI as another which provides a modest flux together with a very high α, the two in these cases being merely acceptable. At any rate, when PSI is very high as in our case, the membrane is of high performance, in desalination by PV.

3.4. Membrane micrograph

Fig. 12 presents a surface micrograph of the membrane fabricated and used in the present work in all the experiments. It is clear that the membrane is rough, in that it contains hills and valleys uniformly distributed all over the surface. Moreover, it contains many pores which are in nano-size. This clarifies the excellent rejection properties of the membrane, since the hydrated salt ions cannot permeate through the nano-pores. In addition, the, non-uniform surface causes the salt ions to flow across the membrane surface, without reaching the recessed portions, and thus are prevented from contacting the pores embedded there. In this way, the salt does not easily permeate through the membrane. On the other hand, as regards the water, it easily diffuses through the membrane, since the membrane is superhydrophilic, owing to the presence of three hydrophilic hydroxyl groups in its anhydroglucose units, which assists in the diffusion of water through the make and break of hydrogen bonds.

The micrograph of the membrane cross section is illustrated in Fig. 13. The figure clarifies the asymmetric nature of the deacetylated membrane, and reveals the gradually increasing pore size from the skin layer downward to the underside in which large voids are apparent, which facilitates the diffusion of water from top to bottom through the membrane by the make and break of hydrogen bonds, formed between each water molecule and hydroxyl ions in the polymer matrix.

Moreover, the matrix itself is porous, and is surrounded by the large voids, thus water is allowed to diffuse easily through the matrix itself, plus through the mini- and macro-pores. Accordingly, the membrane is of outstanding performance as regards flux and salt rejection. In this respect, the membrane's performance exceeds those of all membranes cited in the literature for the dehydration of alcohols [35–37] and breaking of alcohol-water azeotropes [38].

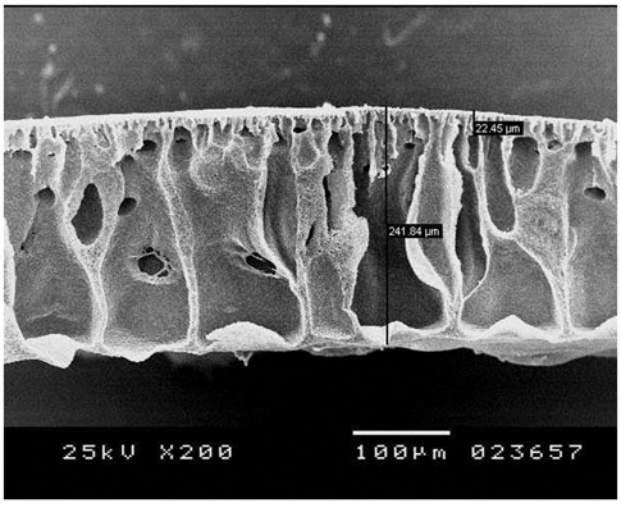

Fig. 13. SEM cross section micrograph of fabricated membrane with magnification of 200×.

Furthermore, it is much better than the very few ones which have been applied to desalination by PV, and which were at much lower feed salt concentrations [16,23,39,40].

3.5. Activation energy

The activation energy (E_a) was determined by plotting ln (J) where J is the flux in l/m^2 h, vs. the reciprocal of Tpv in degrees Kelvin, according to the Arrhenius equation, as shown in Fig. 14, from which E_a is computed from the slope of the best fitting line. It was found that E_a was equal to 31.74, 24.17, 20.89, and 36.15, 25.07, 23.06 at C_i = 15, 45, and 120 for the large and small cell, in respective order, which proves that the cell hydrodynamics is to a great deal affected by the cell configuration, and is of great significance in affecting the flux and salt rejection, of the same membrane. Moreover, the low values of E_a in the present work emphasize the ease with which permeation takes place through the membrane, and the excellent membrane performance.

3.6. Diffusion mass transfer

In this case, the total resistance to diffusion is concentrated in the membrane only and thus K_{ov} can be determined for each different experiment in either cell from Eq. (6) by plotting ln(C_0/C) vs. time in seconds as illustrated in Figs. 15–17. These figures depict the straight lines obtained in the small and large cells at different temperatures for the three concentrations employed in the present work: 15, 45, and 120 g/l in Figs. 15–17, respectively. It is clear from the three figures that the slopes of the best fitting lines obtained increase directly with Tpv, indicating that mass transfer is more rapid at higher temperatures during PV, which is expected. Moreover, it is clear that mass transfer in case of the large cell is faster than in the small cell, which emphasizes the important and pronounced effect of the cell configuration, which in turn affects the hydrodynamics of the flow hydrodynamics within the cell, which was explained earlier (the aspect ratio, cell depth, and liquid velocity determine the hydrodynamics).

The observed linear variation of these three plots justifies the use of Eq. (6). However, the deviation from linearity at small times may be inferred by beginning each experiment with a solute-saturated membrane rather than with a membrane containing a

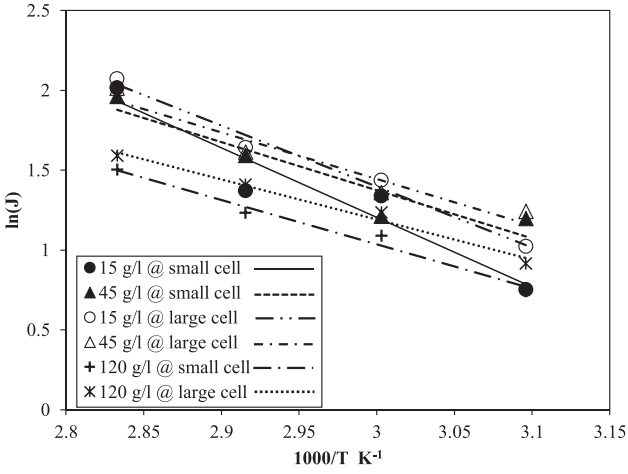

Fig. 14. Plot of ln(flux) l/m^2 h vs. (1/T) K^{-1}.

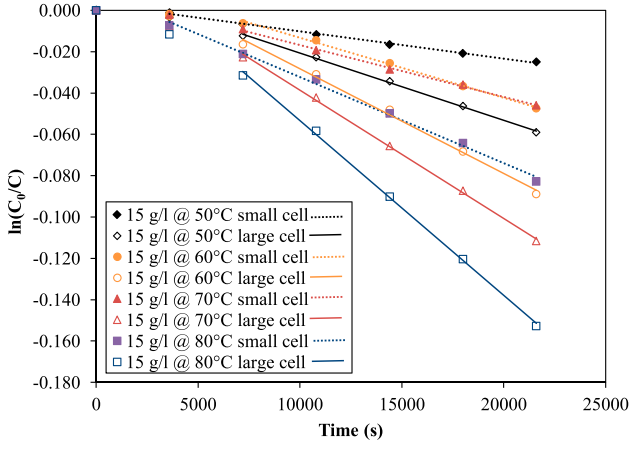

Fig. 15. ln(C_0/C) vs. time at different pervaporate temperatures for small and large cell at 15 g/l feed solution.

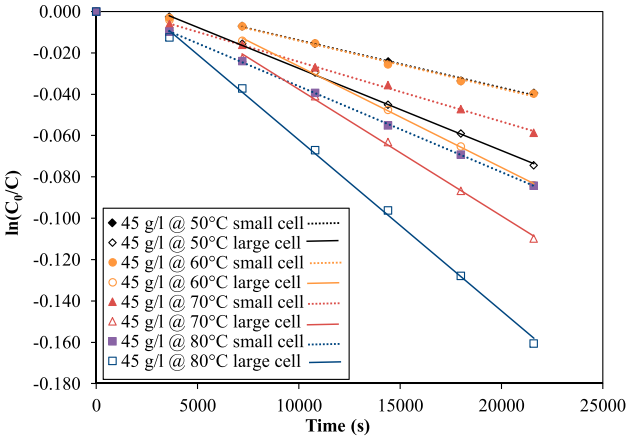

Fig. 16. $\ln(C_0/C)$ vs. time at different pervaporate temperature for small and large cell at 45 g/l feed solution.

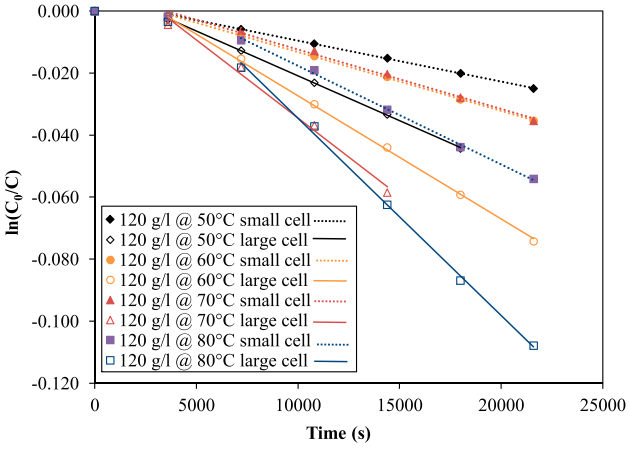

Fig. 17. $\ln(C_0/C)$ vs. time at different pervaporate temperatures for small and large cell at 120 g/l feed solution.

linear concentration gradient [30,41]. Accordingly, this non-linear region and its related time were less reliable than the slope obtained from the data, so we restricted our analysis to the slope of the lines.

Table 1 presents values of J, D_i, K_{ov}, D_s, and P at different C_i (15, 45, and 120 g/l) and different Tpv (50, 60, 70, and 80°C) for the large cell and the small cell, respectively. It is clear that J at each C_i tested increase with Tpv as expected for both cells investigated. In addition, values of J are higher in case of large cell than small cell under identical conditions of C_i and Tpv. Moreover, the values of K_{ov} follow the same trend with C_i and Tpv. It is also noticed from the same table that D_i increases with increase of Tpv for each C_i tested. This observation is justified from Eq. (7) in which D_i is a function of J, δ, and C_i. However, since the same membrane was used for each C_i, at constant C_i, D_i is a function of only J. Therefore, D_i follows the same trend as J and therefore is directly proportional with Tpv. Thus, this increase in D_i is justified.

On the other hand, the salt diffusivity (D_s) does not follow a regular trend as D_i, as noticed from the table, which may be attributed to M_t being different from one experiment to another. This is clarified from Eq. (8) from which D_s was computed depending on the slope of the portion line of plotting M_t/M_∞ vs. $t^{0.5}$. To this end, Bird et al. [42] described the desorption behavior of the NaCl to be largely consistent with that expected from the Fickian diffusion models of the release of solute from a film of uniform thickness. Also, Sagle et al. [43] stated that in many cases, a short induction period was observed, which indicated by the non-linear relationship between the mass uptake and square root of time, to occur at the beginning of each experiment; they ascribed this induction behavior to boundary layer effects before the desorbing solution concentration becomes relatively uniform [44]. However, the salt diffusion coefficients in the study by Sagle et al. [43], were calculated by analyzing the data unaffected by this phenomenon.

From Table 1, the salt permeability (P) is presented at different C_i and Tpv for both large and small cells. It is clear that P depends on K_s (ratio of salt concentration in the pervaporate to that in the feed) and on D_s, from Eq. (10). Thus, since K_s is another way of expressing %SR, the result is that salt permeability is minimum when %SR and D_s are minimum. Accordingly, it is realized from the table that P does not follow a regular pattern since as aforementioned its value relies on K_s and D_s as well as many other factors such as C_i, J, and naturally the membrane morphology. It is worth noting that the lowest P in case of the large cell is achieved in the range of C_i equivalent to sea water of high salt concentration, at 50°C at which $J = 3.46$ l/m^2 h which presents a large saving in energy.

However, in the brackish water range ($C_i = 15$ g/l), the minimum P is at 70°C, but the flux is as high as 5.16 l/m^2 h, which is also very acceptable. On the other hand, if exceptionally high C_i such as 120 g/l is required, such as the case when membrane crystallization is to be applied [45], the minimum permeability took place at 70°C, despite that $J = 4.09$ l/m^2 h; however, %SR in this case was computed to be above 99.7, which is very high.

As regards the small cell, the minimum P was obtained at $C_i = 45$ g/l and 60°C at which J was 3.35 l/m^2 h. In addition, for the sake of comparison, P under the same conditions using the large cell was much higher, with a concomitant higher J of 3.89 l/m^2 h. A final word is that these results regarding P, D_s, K_{ov}, D_i,

and J clarify the effect of the hydrodynamics during pervaporative desalination. Future work is going on to obtain a correlation relating Sherwood, Schmidt, and Reynolds numbers, which will express our results.

4. Conclusion

A superhydrophilic deacetylated CA membrane, of very high performance in desalinating extremely high concentration of aqueous NaCl solutions, by the sweeping air PV technique, was fabricated in this work, by the phase inversion method. Two laboratory-scale cells of different configurations, including aspect ratio, were studied for their effect on the J, %SR, α, and PSI. The cell with higher aspect ratio and deeper cross section of flow was found to give much higher J and α and therefore higher %SR and PSI. It is worth mentioning that the best performance was achieved, using the large cell, at Tpv = 70˚C, for C_i from 15, 45 to 120 g/l, at which the %SR was high and equivalent to a final pervaporate concentration from 0.322, 0.335 to 0.148 g/l, while the fluxes were 5.16, 5.01, and 4.1 l/m^2 h, respectively. Very high initial salt solution concentrations, reaching 120 g/l, were desalinated in a once-through single-stage process, yielding potable water directly, of exceptionally low salinity (99.6 % SR), as well as with very high fluxes, reaching 4.91 l/m^2 h at 80˚C, which are way higher than those reported in the literature for dehydration of alcohols, and desalination by PV, using other membranes, that are fabricated with much more intricate techniques. In this respect, the membrane used in this work is altogether innovated, and is fabricated by a simple, straight-forward, non-complicated way, unlike those reported in the literature, for PV. Activation energies computed from the plot of the Arrhenius equation proved that the membrane offered facile flow to water, while concomitantly restricting salt passage almost totally, under the majority of conditions investigated. Moreover, the values of K_{ov} follow the same trend with C_i and Tpv. It is worth noting that the lowest P in case of the large cell is achieved in the range of C_i equivalent to sea water of high salt concentration, at 50˚C at which J = 3.46 l/m^2 h which presents a large saving in energy.

Acknowledgment

The authors wish to acknowledge the kind support of Science and Technology Development Funds (STDF) of Egypt for funding the research project (ID: 4060) on desalination of sea water through the application of purge-air pervaporation technique.

References

[1] M.C. Duke, J. O'Brien-Abraham, N. Milne, B. Zhu, J.Y.S. Lin, J.C. Diniz da Costa, Seawater desalination performance of MFI type membranes made by secondary growth, Sep. Purif. Technol. 68 (2009) 343–350.
[2] P. Swenson, B. Tanchuk, A. Gupta, W. An, S.M. Kuznicki, Pervaporative desalination of water using natural zeolite membranes, Desalination 285 (2012) 68–72.
[3] G. Clout, Review of CSD-13 Water and Sanitation Decisions in, Statement of the United Nations Industrial Development Organization, UNIDO, New York, NY, 2008.
[4] K.P. Lee, T.C. Arnot, D. Mattia, A review of reverse osmosis membrane materials for desalination—Development to date and future potential, J. Membr. Sci. 370 (2011) 1–22.
[5] R.W. Baker, Membrane Technology and Applications, second ed., John Wiley and Sons, England, 2004.
[6] S.-L. Wee, C.-T. Tye, S. Bhatia, Membrane separation process—Pervaporation through zeolite membrane, Sep. Purif. Technol. 63 (2008) 500–516.
[7] W. An, P. Swenson, L. Wu, T. Waller, A. Ku, S.M. Kuznicki, Selective separation of hydrogen from C_1/C_2 hydrocarbons and CO_2 through dense natural zeolite membranes, J. Membr. Sci. 369 (2011) 414–419.
[8] X. Chen, X. Lin, P. Chen, H. Kita, Pervaporation of ketone/water mixtures through silicalite membrane, Desalination 234 (2008) 286–292.
[9] Q. Liu, R.D. Noble, J.L. Falconer, H.H. Funke, Organics/water separation by pervaporation with a zeolite membrane, J. Membr. Sci. 117 (1996) 163–174.
[10] L.M. Vane, Pervaporation in: H.M. Freeman (Ed.), Standard Handbook of Hazardous Waste Treatment and Disposal, McGraw, New York, NY, 1998, pp. 7.60–67.72.
[11] P.D. Chapman, T. Oliveira, A.G. Livingston, K. Li, Membranes for the dehydration of solvents by pervaporation, J. Membr. Sci. 318 (2008) 5–37.
[12] K. Zhou, Q.G. Zhang, G.L. Han, A.M. Zhu, Q.L. Liu, Pervaporation of water–ethanol and methanol–MTBE mixtures using poly (vinyl alcohol)/cellulose acetate blended membranes, J. Membr. Sci. 448 (2013) 93–101.
[13] S. Xiao, R.Y.M. Huang, X. Feng, Preparation and properties of trimesoyl chloride crosslinked poly(vinyl alcohol) membranes for pervaporation dehydration of isopropanol, J. Membr. Sci. 286 (2006) 245–254.
[14] T. Uragami, H. Matsugi, T. Miyata, Pervaporation characteristics of organic−inorganic hybrid membranes composed of poly(vinyl alcohol-co-acrylic acid) and tetraethoxysilane for water/ethanol separation, Macromolecules 38 (2005) 8440–8446.
[15] Q.G. Zhang, Q.L. Liu, Y. Chen, J.H. Chen, Dehydration of isopropanol by novel poly(vinyl alcohol)−silicone hybrid membranes, Ind. Eng. Chem. Res. 46 (2007) 913–920.
[16] C.H. Cho, K.Y. Oh, S.K. Kim, J.G. Yeo, P. Sharma, Pervaporative seawater desalination using NaA zeolite membrane: Mechanisms of high water flux and high salt rejection, J. Membr. Sci. 371 (2011) 226–238.
[17] S. Khajavi, J.C. Jansen, F. Kapteijn, Production of ultra pure water by desalination of seawater using a hydroxy sodalite membrane, J. Membr. Sci. 356 (2010) 52–57.

[18] S. Khajavi, J.C. Jansen, F. Kapteijn, Performance of hydroxy sodalite membranes as absolute water selective materials under acidic and basic conditions, J. Membr. Sci. 356 (2010) 1–6.
[19] M. Kazemimoghadam, T. Mohammadi, Synthesis of MFI zeolite membranes for water desalination, Desalination 206 (2007) 547–553.
[20] H. Ahn, Y. Lee, Pervaporation of dichlorinated organic compounds through silicalite-1 zeolite membrane, J. Membr. Sci. 279 (2006) 459–465.
[21] E. Korin, I. Ladizhensky, E. Korngold, Hydrophilic hollow fiber membranes for water desalination by the pervaporation method, Chem. Eng. Process. 35 (1996) 451–457.
[22] E. Korngold, E. Korin, Air sweep water pervaporation with hollow fiber membranes, Desalination 91 (1993) 187–197.
[23] S. Ben Hamouda, A. Boubakri, Q.T. Nguyen, M. Ben Amor, PEBAX membranes for water desalination by pervaporation process, High Perform. Polym. 23 (2011) 170–173.
[24] E. Quiñones-Bolaños, H. Zhou, R. Soundararajan, L. Otten, Water and solute transport in pervaporation hydrophilic membranes to reclaim contaminated water for micro-irrigation, J. Membr. Sci. 252 (2005) 19–28.
[25] Z. Xie, D. Ng, M. Hoang, T. Duong, S. Gray, Separation of aqueous salt solution by pervaporation through hybrid organic–inorganic membrane: Effect of operating conditions, Desalination 273 (2011) 220–225.
[26] H.J. Zwijnenberg, G.H. Koops, M. Wessling, Solar driven membrane pervaporation for desalination processes, J. Membr. Sci. 250 (2005) 235–246.
[27] M. Drobek, C. Yacou, J. Motuzas, A. Julbe, L. Ding, J.C. Diniz da Costa, Long term pervaporation desalination of tubular MFI zeolite membranes, J. Membr. Sci. 415–416 (2012) 816–823.
[28] B. Liang, K. Pan, L. Li, E.P. Giannelis, B. Cao, High performance hydrophilic pervaporation composite membranes for water desalination, Desalination 347 (2014) 199–206.
[29] Z. Xie, M. Hoang, D. Ng, C. Doherty, A. Hill, S. Gray, Effect of heat treatment on pervaporation separation of aqueous salt solution using hybrid PVA/MA/TEOS membrane, Sep. Purif. Technol. 127 (2014) 10–17.
[30] A.M. Gronda, S. Buechel, E.L. Cussler, Mass transfer in corrugated membranes, J. Membr. Sci. 165 (2000) 177–187.
[31] H. Yasuda, C.E. Lamaze, L.D. Ikenberry, Permeability of solutes through hydrated polymer membranes. Part I. Diffusion of sodium chloride, Makromolek, Chemie 118 (1968) 19–35.
[32] M.M. Naim, A.A. El-Shafei, A.A. Moneer, M.M. Elewa, Ultrafiltration by a super-hydrophilic regenerated cellulose membrane, Water Pract. Technol. 10 (2015) 337–346.
[33] E. Korngold, E. Korin, I. Ladizhensky, Water desalination by pervaporation with hollow fiber membranes, Desalination 107 (1996) 121–129.
[34] M. Naim, M. Elewa, A. El-Shafei, A. Moneer, Desalination of simulated seawater by purge-air pervaporation using an innovative fabricated membrane, Water Sci. Technol. 72 (2015) 785–793.
[35] S.Y. Hu, Y. Zhang, D. Lawless, X. Feng, Composite membranes comprising of polyvinylamine-poly(vinyl alcohol) incorporated with carbon nanotubes for dehydration of ethylene glycol by pervaporation, J. Membr. Sci. 417–418 (2012) 34–44.
[36] R.P. Pandey, V.K. Shahi, Functionalized silica–chitosan hybrid membrane for dehydration of ethanol/water azeotrope: Effect of cross-linking on structure and performance, J. Membr. Sci. 444 (2013) 116–126.
[37] S.B. Kuila, S.K. Ray, Separation of isopropyl alcohol–water mixtures by pervaporation using copolymer membrane: Analysis of sorption and permeation, Chem. Eng. Res. Des. 91 (2013) 377–388.
[38] W.L. Luyben, Control of a column/pervaporation process for separating the ethanol/water azeotrope, Ind. Eng. Chem. Res. 48 (2009) 3484–3495.
[39] Y.P. Kuznetsov, E.V. Kruchinina, Y.G. Baklagina, A.K. Khripunov, O.A. Tulupova, Deep desalination of water by evaporation through polymeric membranes, Russ. J. Appl. Chem. 80 (2007) 790–798.
[40] P. Swenson, B. Tanchuk, A. Gupta, W. An, S.M. Kuznicki, Pervaporative desalination of water using natural zeolite membranes, Desalination 285 (2012) 68–72.
[41] E.L. Cussler, Diffusion: Mass Transfer in Fluid Systems, third ed., Cambridge University Press, Cambridge, UK, 2009.
[42] R.B. Bird, W.E. Stewart, E.N. Lightfoot, Transport Phenomena, second ed., John Wiley & Sons Inc., New York, NY, 2007.
[43] A.C. Sagle, H. Ju, B.D. Freeman, M.M. Sharma, PEG-based hydrogel membrane coatings, Polymer 50 (2009) 756–766.
[44] J. Crank, G.S. Park, Diffusion in Polymers, Academic Press Inc., New York, NY, 1981.
[45] F. Edwie, T.-S. Chung, Development of simultaneous membrane distillation–crystallization (SMDC) technology for treatment of saturated brine, Chem. Eng. Sci. 98 (2013) 160–172.